

# A NOVEL 3d TRANSITION-METAL ALCOCRUTI HIGH-ENTROPY ALLOY

## NOVE VISOKO ENTROPIJSKE ZLITINE NA OSNOVI 3d SKUPINE PREHODNIH KOVIN

Jiaojiao Yi<sup>1</sup>, Lin Yang<sup>2</sup>, Lu Wang<sup>2</sup>, Mingqin Xu<sup>1\*</sup>

<sup>1</sup> School of Mechanical Engineering, Jiangsu University of Technology, 1801 Zhongwu Road, Zhonglou District, Changzhou 213001, PR China

<sup>2</sup> School of Materials Science and Engineering, Jiangsu University of Technology, 1801 Zhongwu Road, Zhonglou District, Changzhou 212013, PR China

Prejem rokopisa – received: 2020-01-26; sprejem za objavo – accepted for publication: 2021-02-06

doi:10.17222/mit.2021.013

The phase component, microstructure and compressive properties of a novel 3d transition-metal high-entropy alloy, AlCoCrCuTi, in the as-cast and annealed conditions, are investigated. The phases of the as-cast AlCoCrCuTi alloy include primary phase AlCo<sub>2</sub>Ti (L<sub>21</sub>), eutectic structure {AlCo<sub>2</sub>Ti (L<sub>21</sub>) + Al<sub>3</sub>Cr<sub>7</sub> (BCC)} and interdendritic phase AlCu<sub>2</sub>Ti (L<sub>21</sub>). During annealing, the rosette feature of the as-cast AlCo<sub>2</sub>Ti + Al<sub>3</sub>Cr<sub>7</sub> eutectic structure is deteriorated because the lath-like Al<sub>3</sub>Cr<sub>7</sub> changes into a finely divided one. Regarding the mechanical performance, the as-cast alloy exhibits a balanced synergy of hardness (593 ± 37) HV and ultimate strength (745 MPa), while the hardness of the annealed alloy slightly increases, to (647 ± 23) HV, at the expense of the ultimate strength. Moreover, the alloy in both the as-cast and annealed conditions unfortunately display a typically brittle character. The deficiency in elongation might stem from the incorporated diversified brittle and hard phases, such as AlCo<sub>2</sub>Ti + Al<sub>3</sub>Cr<sub>7</sub>.

Keywords: high-entropy alloys, phase structure, microstructure, mechanical properties

V članku avtorji opisujejo raziskave faznih komponent, mikrostrukturo in mehanske lastnosti nove visoko entropijske zlitine na osnovi 3d skupine prehodnih kovin tipa AlCoCrCuTi v litem in toplotno obdelanem stanju. Faze zlitine AlCoCrCuTi v litem stanju primerjajo s primarno fazo AlCo<sub>2</sub>Ti (L<sub>21</sub>), evtektisko strukturo {AlCo<sub>2</sub>Ti (L<sub>21</sub>) + Al<sub>3</sub>Cr<sub>7</sub> (BCC)} in med-dendritno fazo AlCu<sub>2</sub>Ti (L<sub>21</sub>). Po toplotni obdelavi se je rozetasta lita struktura evtektiske faze AlCo<sub>2</sub>Ti + Al<sub>3</sub>Cr<sub>7</sub> poslabšala in spremenila v enotno letvasto strukturo podobno fazi Al<sub>3</sub>Cr<sub>7</sub>. Mehanske lastnosti zlitine v litem stanju kažejo določeno sinergijo med trdoto (593 ± 37) HV in tlačno trdnostjo (745 MPa), medtem ko je po toplotni obdelavi trdota zlitine rahlo narasla (647 ± 23) HV na račun trdnosti. Poleg tega, ne glede na to v kakšnem stanju je zlitina (litem ali toplotno obdelanem), kaže tipičen krhek značaj. Pomanjkanje duktilnosti zlitine je verjetno posledica porazdelitve krhkih in trdih faz, kot sta AlCo<sub>2</sub>Ti + Al<sub>3</sub>Cr<sub>7</sub>.

Ključne besede: visoko entropijske zlitine, fazna struktura, mikrostruktura, mehanske lastnosti

## 1 INTRODUCTION

Mostly due to the vast range of composition combinations and excellent mechanical properties,<sup>1–3</sup> high-entropy alloys (HEAs), usually composed of ≥5 principal elements with the concentration in a range of 5–35 %, <sup>1,2</sup> have attracted considerable attention.<sup>4–8</sup> Among all the reported HEAs, 3d transition-metal (3d TM) HEAs, which commonly contain 4 of 9 of the following elements: Al, Co, Cr, Cu, Fe, Mn, Ni, Ti and V,<sup>9–14</sup> are the most widely studied alloy system. However, of all the alloying combinations, there are just two quinary alloys including Al, Co, Cr and Cu (AlCoCrCuFe, AlCoCrCuNi).<sup>15,16</sup> This indicates that the alloying combinations of AlCoCrCu and Mn/Ti/V remain unexploited.

The AlCoCrCuNi alloy, first reported by Yeh et al.,<sup>15</sup> is constituted by an ordered BCC (B2) phase and an FCC phase. While one of the principal elements, Ni, is substituted by a similar element, Fe, another quinary alloy, AlCoCrCuFe, obtained by Kottada et al.,<sup>16</sup> contains B2 +

FCC + σ (FeCr-containing) phases instead of the B2 + FCC phase of the AlCoCrCuNi alloy. This indicates that a tiny change of the principal elements in a settled AlCoCrCu-based alloy has a strong effect on the alloying phase component.<sup>2,17</sup> Thus, the phase component and subsequent mechanical properties of the unreported alloying combinations of AlCoCrCuX (X = Mn, Ti or V) are worth investigating. Among Mn, Ti and V, the great effects of Ti on mechanical properties, especially the yield strength and ductility, were clearly evidenced in many works.<sup>18–20</sup> For instance, the experimental investigation of the CoCrCuFeNiTi<sub>x</sub> (x values in molar ratio, x = 0, 0.5, 0.8 and 1.0) HEAs by Zhang et al.<sup>18</sup> showed that their alloy series have a simple single-phase FCC solid solution with a high ductility between 21.6–50.2 % when x ≤ 0.5, and the phase component of the FCC + laves phases has a high yield strength of 1042–1272 MPa when 0.5 < x ≤ 1. Similarly, the hardness of Al<sub>0.5</sub>CoCrCuFeNiTi<sub>x</sub> (x = 0–2.0) increases from 220–320 HV for x = 0–0.4 to 320–580 HV for x = 0.4–0.8 and further to 580–650 HV for x = 0.8–1.2, with the phase changing from FCC

\*Corresponding author's e-mail:  
xumingqin3600@163.com (Mingqin Xu)

( $x = 0-0.4$ ) and FCC+BCC ( $x = 0.4-0.8$ ) to FCC+BCC+ $\sigma$  ( $x = 0.8-1.2$ ).<sup>20</sup>

Thus, in this study, considering the significant effect of Ti on the phase component and mechanical properties, Ti was added to AlCoCrCu to fabricate a new 3d TM HEA AlCoCrCuTi. Afterwards, its phase component, microstructure and mechanical properties in the as-cast and annealed conditions were investigated intensively.

## 2 EXPERIMENTAL PART

AlCoCrCuTi ingots were prepared by arc melting the equimolar mixtures of the principal elements. Al, Co, Cr, Cu and Ti were bulk slugs with a purity of 99.99, 99.9, 99.95, 99.95 and 99.9 % ( $x/\%$ ), respectively. The melting process was conducted in a water-cooled copper crucible under a Ti-getter argon atmosphere. To reach the compositional homogeneity, the ingots were re-melted four times, flipped for each melt and kept in the liquid state for 3 min during each melting event. The prepared button was about 8 mm thick and 15 mm in diameter with a shiny surface. Before casting, the ingot was cut by a diamond saw into pieces weighing about 10 g each. The ingot pieces were melted by arc melting and then sucked into a room temperature (RT) cylinder-shaped copper mould with a diameter of 4 mm and a length of 60 mm. The actual alloy composition was characterized by an EDS (Energy Dispersive Spectrometer) as  $Al_{19.7}Co_{20.2}Cr_{20.3}Cu_{19.0}Ti_{20.8}$ , which is very close to the nominal composition. To homogenize the microstructure of an as-cast sample, it was annealed under a vacuum condition at 1673 K for 20 h. Prior to annealing, the sample was wrapped with a 0.1 mm Ta foil to relax the oxidation.

The phase components of the as-cast and annealed alloys were identified using a PANalytical X'Pert X-ray diffractometer,  $CuK_{\alpha}$  radiation and a  $2\theta$  range of  $20-120^{\circ}$ . Microhardness was obtained through a Vickers-microhardness tester (HVS-1000B) used on the

polished cross-sections of the cylinder samples under a load of 50 g for 10 s. The microstructure was analysed using a scanning electron microscope (SEM, Zeiss sigma 500) equipped with an electron backscattered diffraction (EBSD, Oxford) detector. The scan step for the EBSD detection was 2  $\mu m$ , and the scan region covered  $600 \mu m \times 450 \mu m$ .

Compression tests of the cylinder samples (3.7 mm in diameter and  $\approx 5.6$  mm in height) were conducted at RT using a computer-controlled Instron (Instron, Norwood, MA) mechanical testing machine outfitted with silicon carbide dies. The loading direction was parallel to the sample's axis. A constant ramp speed of  $5.6 \times 10^{-3}$  mm/s was applied to the samples, which corresponded to the initial strain rate of  $10^{-3} s^{-1}$ .

## 3 RESULTS

Figure 1 shows XRD patterns of the as-cast and annealed AlCoCrCuTi alloys (a and b) together with those of the as-cast AlCoCrCuNi and as-sintered AlCoCrCuFe alloys (c and d).<sup>11,15,16</sup> Accordingly, a typical B2 (ordered BCC) + FCC dual-phase structure was identified in the as-cast AlCoCrCuNi alloy (see Figure 1c), while an extra FeCr-containing sigma ( $\sigma$ ) phase emerged in the AlCoCrCuFe alloy (Figure 1d). Comparatively, through the Ti incorporation replacing Ni or Fe, the phase components of the currently studied alloy AlCoCrCuTi, regardless of the as-cast or annealed conditions, were clearly identified as two  $L_{21}$  phases ( $L'$  and  $L''$ ) and one BCC phase (Figures 1a and 1b). Note that identical XRD patterns obtained through annealing implied that AlCoCrCuTi exhibits a promising thermal stability. According to JCPDS cards, the BCC phase is approximately consistent with the stoichiometric compounds of  $Al_3Cr_7$  with a lattice parameter of 295.5 pm. In addition, the diffraction peaks of the two  $L_{21}$  ( $L'$  and  $L''$ ) phases corresponded to the peaks of  $AlCu_2Ti$  and  $AlCo_2Ti$ , respectively. Their lattice parameters were determined to be around  $a = 598.8$  pm ( $L'$ ) and 582.9 pm ( $L''$ ). The formation of the  $L_{21}$  phases might have stemmed from the high bonding strength among Al, Ti and Cu/Co, which is similar to  $AlNi_2Ti$  in  $AlCoCrCuNiTiY_x$  ( $x = 0.5, 0.8, 1$ ).<sup>21</sup>

Figure 1 shows X-ray diffraction patterns of the as-cast and annealed AlCoCrCuTi alloys (a and b) together with those of the as-cast AlCoCrCuNi and as-sintered AlCoCrCuFe alloys (c and d).<sup>11,15,16</sup> B,  $L'$  and  $L''$  stand for BCC and two  $L_{21}$  phases; B2 and F stand for ordered BCC and FCC phases.

The micrographs of the as-cast and annealed AlCoCrCuTi alloys are shown in Figures 2a to 2d, respectively. For the as-cast alloy, the microstructure is composed of a primary phase (marked as 1 in Figure 2b), a rosette-eutectic organization (2) and an interdendritic phase (3). The primary phase is randomly stacked into an overall formation with an average width of about 10  $\mu m$ . At the edges of the primary phase, the

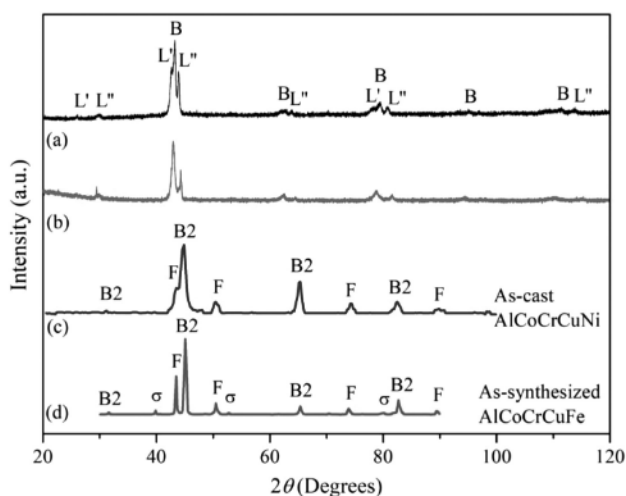


Figure 1: X-ray diffraction patterns

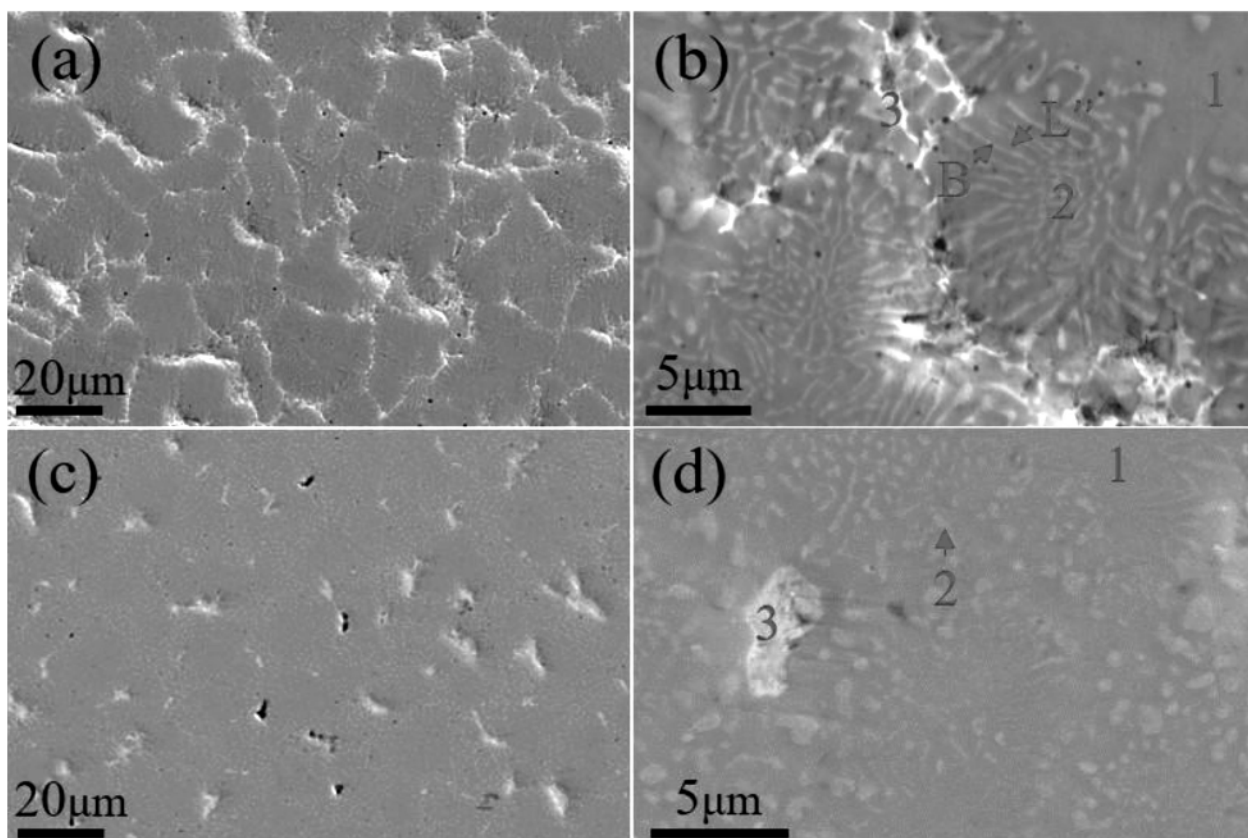


Figure 2: SEM micrographs of the microstructure of the AlCoCrCuTi HEA: a), b) as-cast and c), d) annealed conditions

rosette-eutectic structure seems to enclose the primary phase. To be sophisticated, the rosette-eutectic structure consists of two phases: a grey phase similar to the primary phase and a light phase. In addition, a continuous bright and strip-like phase covering the remaining regions is found to be an interdendritic phase (bright part as 3).

To profile the compositional distribution and establish the link between the diverse regions and the phase analysis, EDS mapping was carried out in the present work as shown in Figures 3a to 3f. As a supplement to the EDS mapping, specific chemical compositions of all regions were extracted from the EDS analysis, as summarized in Table 1. Accordingly, we conclude that the primary regions are mainly enriched with Co and the ro-

sette-eutectic regions are constituted by two distinct morphologies of the light-grey region rich in Cr and grey region rich in Co. Besides, the great majority of Cu segregates in the interdendritic regions, while Ti distributes uniformly in the rest of the regions (i.e., the primary and eutectic regions) and Al distributes evenly in all the regions. According to the phase analysis, it is suggested that the interdendritic regions correspond to the AlCu<sub>2</sub>Ti L' phase and the primary phase regions correspond to the AlCo<sub>2</sub>Ti-like L'' phase.

The rosette-eutectic organization (2) consists of the Al<sub>3</sub>Cr<sub>7</sub> BCC phase (B) and AlCo<sub>2</sub>Ti L<sub>21</sub> phase (L''), and the pre-eutectic phase is the AlCo<sub>2</sub>Ti L<sub>21</sub> phase, which is in agreement with the as-cast AlTiCr<sub>x</sub>FeCoNiCu (x = 0.5–2.5) alloys.<sup>21,22</sup> Moreover, to provide evidence of the

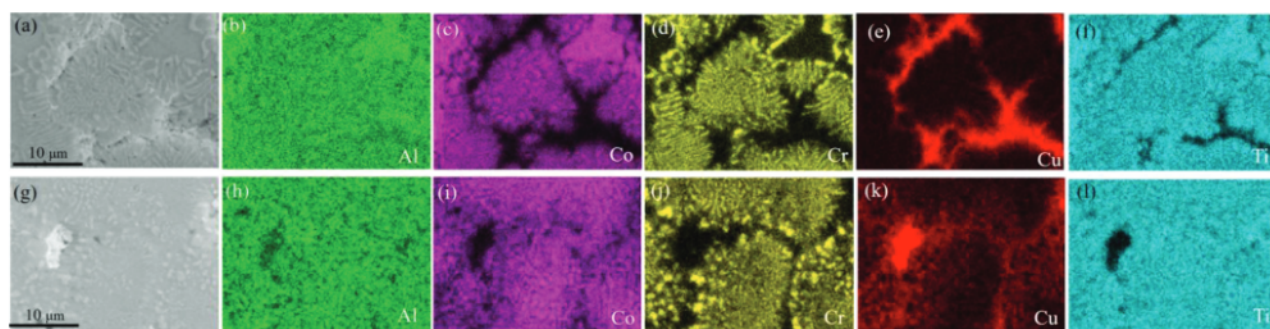


Figure 3: SEM images and the corresponding mapping of Al, Co, Cr, Cu and Ti, (a–f) the as-cast and (g–l) annealed AlCoCrCuTi alloys

**Table 1:** Quantitative chemical analysis of AlCoCrCuTi samples in the as-cast and annealed conditions (x%)

	region	Al	Co	Cr	Cu	Ti
AC	Primary phase	13.8 ± 0.9	32.6 ± 6.6	16.1 ± 6.6	12.2 ± 3.9	25.3 ± 1.8
	Eutectic	9.9 ± 0.6	19.7 ± 0.3	35.6 ± 3.2	13.8 ± 1.7	21 ± 0.7
	Interdendritic	13.4 ± 0.4	3.4 ± 0.8	3.8 ± 0.9	61.2 ± 3.5	18.2 ± 4.2
A	Primary phase	12.7 ± 0.7	26.1 ± 2.1	22.1 ± 3.9	16.2 ± 4.3	22.9 ± 1.1
	Eutectic	7.9 ± 0.7	13.1 ± 1.2	48.2 ± 4.3	14.1 ± 1.5	16.7 ± 1.2
	Interdendritic	9.7 ± 0.8	3.0 ± 0.1	8.4 ± 5.6	76.2 ± 5.1	2.9 ± 0.4

phase component, an EBSD test was conducted and a representative EBSD mapping of the as-cast AlCoCrCuTi alloy is shown in **Figure 4**. **Figures 4a** and **4b** include an inverse pole figure (IPF) map and the standard stereographic triangle, respectively. Hereby, more than half includes the L<sub>21</sub> phases, which strongly indicates that the Ti incorporation is beneficial to the formation of an L<sub>21</sub> phase. Besides, the alloy exhibits typically equiaxed grains with a relatively random crystallographic orientation, and the average grain size is around 100 μm.

Likewise, the morphology of the annealed alloy also consists of three distinct regions (**Figures 2c** and **2d**), which are solidly confirmed by the three distinctly compositional regions of the EDS mapping, shown in **Figures 3g** to **3l**. Accordingly, it can be figured out that the bright interdendritic regions are still enriched with Cu, while the light-grey regions of the original eutectic are enriched with Cr. However, the Cu concentration in them significantly increases from 62.8 % to 71.1 %, which might stem from the exclusion of the other principal elements during the annealing process. Moreover, the original rosette-like eutectic structure seems to become deteriorated via annealing as the bright part corresponding to the Al<sub>3</sub>Cr<sub>7</sub> BCC phase in the as-cast alloy was broken into the small particles (**Figure 2d**). These changes indicate that the as-cast alloy is not in the equilibrium state, proving that post-process annealing is necessary for establishing the phase equilibrium.<sup>8</sup> However, the standard thermal treatment, ensuring that equilibrium is achieved is still lacking, which needs to be comprehensively investigated in spite of the findings of the present research.

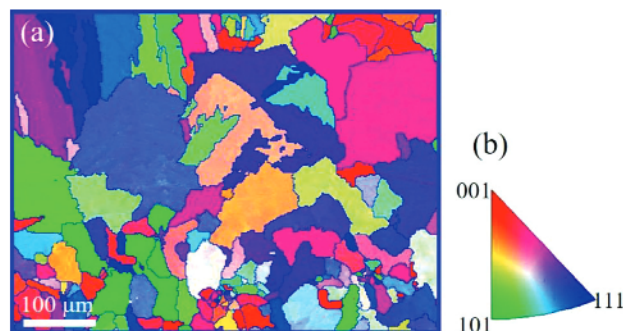


**Figure 4:** EBSD mapping of typical as-cast microstructure characteristics: a) inverse pole figure (IPF) map, b) standard stereographic triangle illustrating random grain orientations

The engineering stress  $\sigma$ , vs. engineering strain  $\epsilon$ , curves of the as-cast and annealed AlCoCrCuTi alloys are shown in **Figure 5**. Their mechanical properties, such as ultimate compressive strength  $\sigma_b$ , elongation  $\delta$ , and microhardness HV<sub>0.05</sub> for both states are summarized in **Table 2**. It is seen that via annealing, the hardness increases from (593 ± 37) HV for the as-cast alloy to (647 ± 23) HV for the annealed alloy, while the ultimate strength decreases from 745 MPa for the as-cast alloy to 265 MPa for the annealed one. Through annealing, the rosette feature of the as-cast AlCo<sub>2</sub>Ti + Al<sub>3</sub>Cr<sub>7</sub> eutectic structure deteriorates since the lath-like Al<sub>3</sub>Cr<sub>7</sub> changes into a finely-divided structure; as a result, the eutectic regions are strengthened with the precipitation strengthening of the fine Cr-rich Al<sub>3</sub>Cr<sub>7</sub> phase (**Figure 2d**). This was seen as the main reason for the enhanced hardness of the annealed alloy, which is strongly supported by a similar strengthening mechanism in some HEAs (for example, AlTiCr<sub>x</sub>FeCoNiCu alloys<sup>22</sup>): a certain amount of the fine BCC phase distributed evenly in the eutectic structure can significantly enhance their microhardness. However, the alloy in both the as-cast or annealed conditions unfortunately display a typically brittle character.

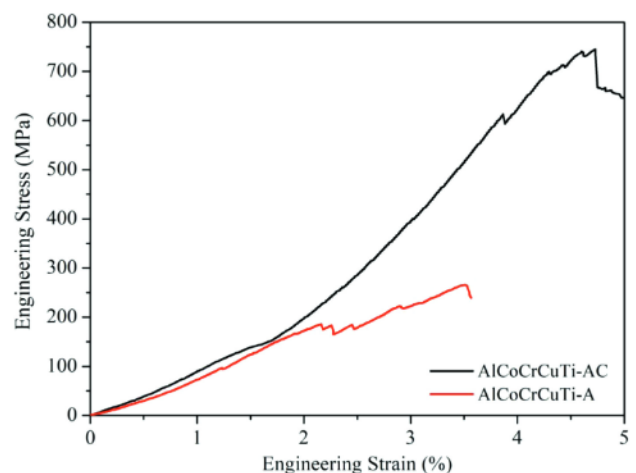


**Figure 5:** Engineering stress vs. engineering strain compression curves of the as-cast and annealed AlCoCrCuTi HEA

**Table 2:** Ultimate compressive strength  $\sigma_b$ , elongation  $\delta$  and microhardness HV<sub>0.05</sub> of the as-cast and annealed AlCoCrCuTi alloys

Composition	$\sigma_b$ (MPa)	$\delta$ (%)	HV
AlCoCrCuTi -AC	745	0.4	593 ± 37
AlCoCrCuTi -A	265	0.2	647 ± 23

The deficiency of ductility might stem from the incorporated diversified brittle and hard phases, such as  $\text{AlCo}_2\text{Ti}$  +  $\text{Al}_3\text{Cr}_7$ , due to which the yield strength might be sensitive to the casting quality. That is to say, the casting drawback formed during the casting process might play a vital role, affecting the intrinsic yield strength.

#### 4 CONCLUSIONS

In summary, the phase constituent, microstructures and mechanical properties of a novel 3d transition-metal HEA,  $\text{AlCoCrCuTi}$ , were investigated using XRD, SEM (equipped with EBSD) and a mechanical testing machine. The following conclusions were reached:

1) The phases of the as-cast  $\text{AlCoCrCuTi}$  alloy are composed of primary phase  $\text{AlCo}_2\text{Ti}$  ( $L_{21}$ ), eutectic structure  $\{\text{AlCo}_2\text{Ti}$  ( $L_{21}$ ) +  $\text{Al}_3\text{Cr}_7$  (BCC) $\}$  and interdendritic phase  $\text{AlCu}_2\text{Ti}$  ( $L_{21}$ ).

2) During annealing, the rosette feature of the as-cast  $\text{AlCo}_2\text{Ti}$  +  $\text{Al}_3\text{Cr}_7$  eutectic structure deteriorates because the lath-like  $\text{Al}_3\text{Cr}_7$  changes into a finely divided structure.

3) The as-cast alloy exhibits a balanced synergy of the hardness ( $593 \pm 37$ ) HV and ultimate strength (74 MPa), while the hardness of the annealed alloy slightly increases, to ( $647 \pm 23$ ) HV, at the expense of the ultimate strength.

#### Acknowledgment

The financial support from the Natural Science Foundation of the Jiangsu Province (Grant No. BK20181047) and Natural Science Research of Jiangsu Higher Education Institutions (Grant No. 18KJB430012) are gratefully acknowledged.

#### 5 REFERENCES

- D. B. Miracle, High entropy alloys as a bold step forward in alloy development, *Nat. Commun.*, 10 (2019), 1805, doi:10.1038/s41467-019-09700-1
- N. D. Stepanov, D. G. Shaysultanov, G. A. Salishchev, M. A. Tikhonovsky, E. E. Oleynik, A. S. Tortika, O. N. Senkov, Effect of V content on microstructure and mechanical properties of the  $\text{CoCrFeMnNiV}_x$  high entropy alloys, *J. Alloys Compd.*, 628 (2015), 170–185, doi:10.1016/j.jallcom.2014.12.157
- Y. Dong, Y. Lu, J. Kong, J. Zhang, T. Li, Microstructure and mechanical properties of multi-component  $\text{AlCrFeNiMo}_x$  high-entropy alloys, *J. Alloys Compd.*, 573 (2013), 96–101, doi:10.1016/j.jallcom.2013.03.253
- R. R. Eleti, T. Bhattacharjee, A. Shibata, N. Tsuji, Unique deformation behavior and microstructure evolution in high temperature processing of  $\text{HfNbTaTiZr}$  refractory high entropy alloy, *Acta Mater.*, 171 (2019), 132–145, doi:10.1016/j.actamat.2019.04.018
- J. Li, Q. Fang, B. Liu, Y. Liu, Transformation induced softening and plasticity in high entropy alloys, *Acta Mater.*, 147 (2018), 35–41, doi:10.1016/j.actamat.2018.01.002
- I. Basu, V. Ocelik, J. T. M. De Hosson, Size dependent plasticity and damage response in multiphase body centered cubic high entropy alloys, *Acta Mater.*, 150 (2018), 104–116, doi:10.1016/j.actamat.2018.03.015
- K. F. Quiambao, S. J. McDonnell, D. K. Schreiber, A. Y. Gerard, K. M. Freedy, P. Lu, J. E. Saal, G. S. Frankel, J. R. Scully, Passivation of a corrosion resistant high entropy alloy in non-oxidizing sulfate solutions, *Acta Mater.*, 164 (2019), 362–376, doi:10.1016/j.actamat.2018.10.026
- D. B. Miracle, O. N. Senkov, A critical review of high entropy alloys and related concepts, *Acta Mater.*, 122 (2017), 448–511, doi:10.1016/j.actamat.2016.08.081
- B. Cantor, I. T. H. Chang, P. Knight, A. J. B. Vincent, Microstructural development in equiatomic multicomponent alloys, *Mater. Sci. Eng. A*, 375–377 (2004), 213–218, doi:10.1016/j.msea.2003.10.257
- J. W. Yeh, S. K. Chen, J. Y. Gan, S. K. Chen, T. T. Shun, C. H. Tsau, S. Y. Chang, Formation of simple crystal structures in  $\text{Cu-Co-Ni-Cr-Al-Fe-Ti-V}$  alloys with multiprincipal metallic elements, *Metall. Mater. Trans. A*, 35A (2004), 2533–2536, doi:10.1007/s11661-006-0234-4
- J. W. Yeh, S. K. Chen, S. J. Lin, J. Y. Gan, T. S. Chin, T. T. Shun, C. H. Tsau, S. Y. Chang, Nanostructured high-entropy alloys with multiple principal elements: novel alloy design concepts and outcomes, *Adv. Eng. Mater.*, 6 (2004), 299–303, doi:10.1002/adem.200300567
- Y. Zhang, T. T. Zuo, Z. Tang, M. C. Gao, K. A. Dahmene, P. K. Liaw, Z. P. Lu, Microstructures and properties of high-entropy alloys, *Prog. Mater. Sci.*, 61 (2014), 1–93, doi:10.1016/j.pmatsci.2013.10.001
- C. J. Tong, M. R. Chen, J. W. Yeh, S. J. Lin, S. K. Chen, T. T. Shun, S. Y. Chang, Mechanical performance of the  $\text{Al}_3\text{CoCrCuFeNi}$  high-entropy alloy system with multi-principal elements, *Metall. Mater. Trans. A*, 36A (2005), 1263–1271, doi:10.1007/s11661-005-0218-9
- M. H. Tsai, J. W. Yeh, High-entropy alloys: a critical review, *Mater. Res. Lett.*, 2 (2014) 3, 107–123, doi:10.1080/21663831.2014.912690
- J. W. Yeh, S. Y. Chang, Y. D. Hong, S. K. Chen, S. J. Lin, Anomalous decrease in X-ray diffraction intensities of  $\text{Cu-Ni-Al-Co-Cr-Fe-Si}$  alloy systems with multi-principal elements, *Mater. Chem. Phys.*, 103 (2007) 1, 41–46, doi:10.1016/j.matchemphys.2007.01.003
- S. Praveen, B. S. Murty, R. S. Kottada, Alloying behavior in multi-component  $\text{AlCoCrCuFe}$  and  $\text{NiCoCrCuFe}$  high entropy alloys, *Mater. Sci. Eng. A*, 534 (2012), 83–89, doi:10.1016/j.msea.2011.11.044
- J. Y. He, W. H. Liu, H. Wang, Y. Wu, Z. P. Lu, Effects of Al addition on structural evolution and tensile properties of the  $\text{FeCoNiCrMn}$  high-entropy alloy system, *Acta Mater.*, 62 (2014), 105–113, doi:10.1016/j.actamat.2013.09.037
- X. F. Wang, Y. Zhang, Y. Qiao, G. L. Chen, Novel microstructure and properties of multicomponent  $\text{CoCrCuFeNiTi}_x$  alloys, *Intermetallics*, 15 (2007) 3, 357–362, doi:10.1016/j.intermet.2006.08.005
- Y. J. Zhou, Y. Zhang, Y. L. Wang, G. L. Chen, Solid solution alloys of  $\text{AlCoCrFeNiTi}_x$  with excellent room-temperature mechanical properties, *Appl. Phys. Lett.*, 90 (2007) 18, 181904, doi:10.1063/1.2734517
- M. R. Chen, S. J. Lin, J. W. Yeh, S. K. Chen, C. P. Tu, Microstructure and properties of  $\text{Al}_{0.5}\text{CoCrCuFeNiTi}_x$  ( $x=0-2.0$ ) high-entropy alloys, *Mater. Trans.*, 47 (2006) 5, 1395–1401, doi:10.2320/matertrans.47.1395
- Z. Hu, Y. Zhan, G. Zhang, J. She, C. Li, Effect of rare earth Y addition on the microstructure and mechanical properties of high entropy  $\text{AlCoCrCuNiTi}$  alloys, *Mater. Des.*, 31 (2010) 3, 1599–1602, doi:10.1016/j.matdes.2009.09.016
- A. Li, D. Ma, Q. Zheng, Effect of Cr on Microstructure and Properties of a Series of  $\text{AlTiCr}_x\text{FeCoNiCu}$  High-Entropy Alloys, *J. Mater. Eng. Perform.*, 23 (2014) 4, 1197–1203, doi:10.1007/s11665-014-0871-5